Droplet squeezing through a narrow constriction: Minimum impulse and critical velocity

Zhifeng Zhang, Corina Drapaca, Xiaolin Chen, and Jie Xu

Citation: Physics of Fluids **29**, 072102 (2017); doi: 10.1063/1.4990777
View online: http://dx.doi.org/10.1063/1.4990777
View Table of Contents: http://aip.scitation.org/toc/phf/29/7
Published by the American Institute of Physics

Droplet squeezing through a narrow constriction: Minimum impulse and critical velocity

Zhifeng Zhang,[1,a)] Corina Drapaca,[1] Xiaolin Chen,[2] and Jie Xu[3]
[1]*Department of Engineering Science and Mechanics, The Pennsylvania State University, State College, Pennsylvania 16802, USA*
[2]*School of Engineering and Computer Science, Washington State University, Vancouver, Washington 98686, USA*
[3]*Department of Mechanical and Industrial Engineering, University of Illinois at Chicago, Chicago, Illinois 60607, USA*

(Received 10 January 2017; accepted 15 June 2017; published online 7 July 2017)

Models of a droplet passing through narrow constrictions have wide applications in science and engineering. In this paper, we report our findings on the minimum impulse (momentum change) of pushing a droplet through a narrow circular constriction. The existence of this minimum impulse is mathematically derived and numerically verified. The minimum impulse happens at a critical velocity when the time-averaged Young-Laplace pressure balances the total minor pressure loss in the constriction. Finally, numerical simulations are conducted to verify these concepts. These results could be relevant to problems of energy optimization and studies of chemical and biomedical systems. *Published by AIP Publishing.* [http://dx.doi.org/10.1063/1.4990777]

I. INTRODUCTION

A droplet passing through a narrowly constricted channel is one of the most commonly used soft matter models. It has wide applications in natural and life sciences and engineering, with examples ranging from basic biological investigations to microfluidic cell-based devices to water-oil emulsion systems. A brief overview of applications of this model is summarized in Table I.

Such a model is a fundamental unit for many complex fluid systems as can be seen in Table I. The size of the droplet in these applications varies from micrometers to millimeters, which is at the continuum mechanics level. Within these applications, one common physical process is the transport of a soft particle through a constriction with the particle being a solid, a liquid, or a viscoelastic material. Due to the strong interactions between the droplet and the constricted channel, the interfacial dynamics, forces, and energy conversion during the transient process are important aspects that need to be investigated.

In this study, we will focus on the physical model of a Newtonian fluid droplet squeezing through a constriction. Three main components are involved in the process: (1) a droplet, (2) an immiscible carrier fluid, and (3) a constricted channel with characteristic dimension smaller than the droplet diameter. From fluid dynamics point of view, this is a multiphase-flow-under-confinement problem.[11] Recent understandings of this physical process are summarized as follows.

(1) Forces: Past studies have mainly focused on pressure changes with respect to droplet deformation during the squeezing process. For a constant-flow-rate case, time-dependent pressure signatures were obtained in our recent studies.[6,12] Two main competing forces within the system are the surface tension force and the static pressure force. The Young-Laplace equation[13] is often used to quantify the surface tension force, which can then be used to predict a critical passing pressure (or minimum force) for a droplet squeezing through a constriction in a quasi-static state by balancing the static pressure force and the surface tension force.[14,15] However, in a transient process, the simple balance between the surface tension and static pressure forces is insufficient to fully describe the process dynamics.[16] We need to consider the contributions from the dynamic pressure and shear stresses. Supporting studies have been conducted for the pressure signature of a droplet passing through a micro-confinement with time lapse for different cross sections[6,17] and the highest critical pressure at the corresponding critical velocity.[16]

(2) Energies: The kinetic energy of the fluids is converted to (when the droplet enters the constriction) and from (when the droplet exits the constriction) the interfacial energy of the droplet, with viscous dissipations that include the major loss along the channel and minor losses at the constriction inlet and expansion outlet. With the increase of inlet velocity, viscous losses become more important. For example, the major loss increases linearly with velocity and the minor losses increase quadratically with velocity.[18] Besides, the adhesion energy decreases the critical passing pressure;[19] the shear energy determines the dispersed-phase deformation;[20] and the radii of the constriction and the droplet provide the main energy barrier of squeezing through.[21]

a)Email: zfzhang@psu.edu

TABLE I. Applications of a droplet passing through a constriction.

Field	Applications	Reference
Biology	Cancer cell metastasis	1
	Capillary blockage	2
	Ischemic disease	3
Lab-on-a-chip	Micro-pipette	4
	Drug delivery	5
	Cell detection	6
	Biomaterial test	7
Chemical engineering	Oil/water emulsions	8
	Ultrafiltration	9
	Enhanced oil recovery	10

(3) Numerical simulations: Numerical studies provide predictive results and guidance for experiments such as channel geometry selections and pressure signature prediction.[1] Numerical methods commonly used in multiphase flow simulations include the Volume of Fluid (VOF) method,[6,16] the Smoothed Particle Hydrodynamics (SPH) method,[22] the front tracking method,[23] the Lattice-Boltzmann method (LBM),[24] the Immersed Boundary Method (IBM),[25,26] and the multiscale coarse-grain method.[27] The main technical challenge in numerical simulations is the tracking of the interface between the two immiscible liquids: droplet and carrier fluid. The VOF method solves the surface tracking problem represented by governing equations consisting of mass and momentum balance for both the droplet and the surrounding fluid. It is one of the most flexible and efficient methods with a good mass conservation property.[28] Also, it is one of the most widely used and validated methods.[29] The VOF method has been used to study either the single-droplet model or the compound-droplet model.[12]

To transport a droplet at a constant velocity through a constriction, the applied pressure must vary in time and exists in the form exhibiting a pulsatile feature. In this process, large deformation of the droplet exists under strong impact between the droplet and the solid channel. Most recent research has focused on modeling the motion-deformation,[30] constitutive-deformation,[31,32] velocity-pressure,[16] and geometry-pressure relations.[6] An analytical optimization of this transport process can help us understand applications like biomaterial transport, enhanced oil recovery, etc., along a micro-channel with a non-uniform cross-sectional area. Mass, energy, and momentum are the physical quantities that play essential roles in the transport process. In particular, momentum is an important parameter in collision and impact problems. The impulse or momentum change, which is the product between applied force and impact time, has not yet been studied for the problem of a droplet squeezing system. Such a study can shed light on various more complex flow situations such as flows in porous media with relevance to oil recovery.

In this paper, we focus on the momentum change of squeezing a droplet through a constricted channel. Based on a force decomposition, we first analytically estimate the global minimum of momentum change required for squeezing a droplet at different velocities. Later, numerical simulations are conducted to prove these concepts. Our results provide a deeper understanding of the droplet penetration and impact dynamics.

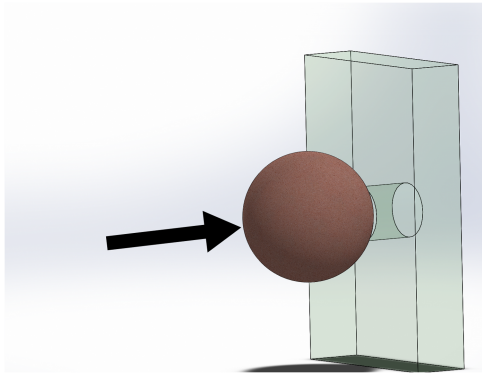

FIG. 1. Sketch of squeezing a Newtonian fluid droplet through a circular constriction in a rigid channel with sudden contraction and expansion.

II. MODEL DESCRIPTION

A mechanical model of a droplet passing through a circular constricted channel is sketched in Fig. 1. In our model, the system is composed of a droplet made of an incompressible Newtonian fluid, a carrier Newtonian fluid, and a narrow circular constricted channel with finite length. In this study, we focus on droplets with a size comparable to that of the constricted channel. To make it applicable to a wide range of applications, the droplet is assumed to have a micro-scale characteristic length scale, on the order of 1-1000 μm. To quantify the model, the geometry and parameters used in analytical and numerical studies are illustrated in Fig. 2. The dynamic viscosity of the droplet is assumed to be the same as that of the carrier fluid, $\eta = 0.001$ Pa s. By this setting, we neglect the viscosity induced pressure inside the droplet, in a low viscosity oil droplet/cell or soft particle studies. A detailed explanation of parameters can be found in the Nomenclature. The droplet is assumed to be squeezed under a constant flow rate condition with a constant outlet pressure. Three important stages are marked as (1) initial contact with the droplet on the side of constriction, (2) a critical pressure point when the advancing length inside the constriction equals the radius of constriction channel, R_C, and (3) droplet out with all volume of the droplet on the right side of the constriction.

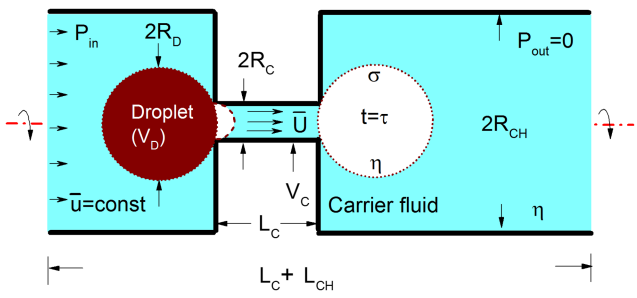

FIG. 2. Geometry and parameters for a droplet squeezing through a narrow constriction.

III. ANALYTICAL FRAMEWORK

A. Characteristic impact time

At low velocity, the droplet is assumed to be in the single-phase transportation regime in the constriction. For a single-phase fluid flow through a channel, the volume flow rate ($\dot{V}_T$) can be expressed using the mass conservation, $\dot{V}_T = \frac{V_T}{t} = \frac{V_D+V_C}{\tau} = \overline{U}A_C$. Here, V_T is the total volume of fluid transported, V_D is the volume of the droplet (assumed constant), V_C is the volume of the constriction, $\overline{U}$ is the average velocity of the flow in the constriction, and A_C is the cross-sectional area of the constriction, τ is the transit time duration defined as the time difference between the beginning and the ending of the droplet-wall contact.[6] Assuming that the operational flow velocity is not significantly high so as to trigger the co-flow of the droplet and carrier fluid in the constriction, we may consider the droplet to be well contacted with the constriction wall during the transport process, i.e., there is no gap formed between the droplet and wall. Under this assumption, we may analytically derive the momentum and the corresponding minimum impulse critical velocity considering only a simple flow in the constriction. Thus, the transit time through the constriction can be expressed as

$$\tau = (V_D + V_C)/\overline{U}A_C. \quad (1)$$

From our numerical simulations, we observe a "pressure rebound" signal at the time of droplet detaching from the constriction. It is a small pressure oscillation labelled as "droplet out" at time τ in Fig. 3. This pressure rebound is induced by the velocity difference between the carrier fluid and the droplet interface recovery. For the time $t < \tau/2$, the carrier liquid pushes the droplet into the channel and the kinetic energy of the flow is stored in the interface. For $t > \tau/2$, the surface energy of the droplet releases and the net surface tension pulls the droplet out of the channel. Consequently, the minimum impulse needed in the flow to complete the entire process is equal to the change in momentum of the droplet before time reaches the characteristic impact time of $T = \tau/2$.

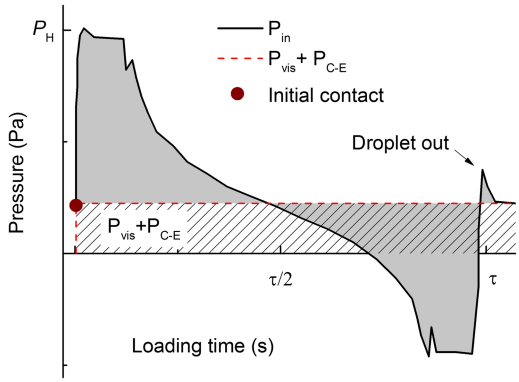

FIG. 3. A decomposition of the inlet pressure in the un-constricted part of the channel-loading time curve for a droplet passing through the constriction.

B. Pressure decomposition

The chamber inlet pressure (P_{in}) is a function of time and the average inlet velocity in the un-constricted channel. According to previous studies,[6] a typical P_{in} $(\overline{u}, t)$-loading time curve (bold solid) is plotted in Fig. 3. As can be seen, after the initial contact between the droplet and the constriction wall, the P_{in} inlet pressure increases very quickly because the curvature of the droplet front cap inside the constriction increases dramatically. As shown in the line-shaded area of Fig. 3, the region below the red dashed line is the constant term induced by the background pressure, which is the sum of viscous term along the channel and the constriction and expansion pressure loss ($P_{vis} + P_{C-E}$). The gray-shaded area is the time integral of surface tension contribution (P_{sur}). An important point in the dynamic curve is the pressure rebound point marked as "droplet out," after which the pressure returns to the background pressure. Corresponding to Table II, pressure terms are labelled in Fig. 3.

TABLE II. The principal pressure components in the system for a sudden circular contraction-and-expansion structure.

Order	Pressure term	Expression	Remark
0th	Time-averaged surface tension term, $(\overline{P}_{sur})$	$\alpha \times 2\sigma(1/R_C - 1/R_D)$	α is a time-averaged parameter over a time range between 0 and $\tau/2$. σ is the surface tension coefficient; R_C is the constriction radius; R_D is the droplet radius
1st	Pressure drop due to viscous effects along the channel, (P_{vis})	$\frac{8\eta L_C}{R_C^2}\overline{U} + \frac{\gamma 8\eta L_{CH}}{R_{ch}^2}\overline{U}$	L_{C} is the length of the constricted channel; L_{CH} is the entrance/exit length of the un-constricted channel; R_{C} is the radius of the constriction; R_{CH} is the entrance/exit radius of the un-constricted channel; η is the viscosity of the carrier fluid
2nd	Pressure drop due to contraction and expansion, (P_{C-E})	$(K_E + K_C)\frac{\rho\overline{U^2}}{2}$	K_C and K_E are the contraction and the expansion coefficients, respectively; ρ is the density of the carrier fluid. For a sudden contraction and expansion, $K_E + K_C = 1.5$

In this paper, we introduce a time-averaged coefficient for the surface tension term to describe the dynamic impact between the droplet and the channel wall. The time-averaged coefficient is defined as $\alpha = \frac{1}{TP_{CR}} \int_0^T P_{sur}(t)dt$. It is the time integration of the dynamic surface tension term $[P_{sur}(t)]$ within a characteristic impact time of T = $\tau/2$ over the product of the Young-Laplace critical pressure given in Eq. (2).

As seen in Figs. 2 and 3, the critical pressure is reached when the droplet front forms a hemispherical cap in the constriction. Assuming that the pressure inside the droplet is uniform, by applying the Laplace law to the front of the droplet (small hemispherical cap with a radius R_C inside the constriction)-carrier fluid (can get the first term $1/R_C$) and the tail of droplet (large spherical cap R_D outside the constriction)-carrier fluid (can get the second term $-1/R_D$), respectively, we can get the simplified form of Young-Laplace critical pressure,

$$P_{CR} = 2\sigma \left(\frac{1}{R_C} - \frac{1}{R_D} \right). \tag{2}$$

Here, P_{CR} is the pressure difference between the upstream (front) and downstream (back) ends, σ is the surface tension coefficient of droplet-carrier fluid, R_C is the radius of the constriction, and R_D is the radius of the un-deformed droplet. This term is generated due to the surface tension at the droplet-carrier fluid interface. Among the three pressure terms, it is the base of the 0th order pressure term (with respect to operation velocity). Strictly speaking, the averaged-surface tension term in Table II also changes with the operation velocity and time. However, α changes very slowly with the operation velocity.

As noticed, we assume the droplet as a Newtonian viscous fluid in this study. For a deformable particle/cell, elastic properties can be taken into account by using the concept of "equivalent surface tension." For example, it is possible to rewrite Eq. (2) by $\sigma_{eq} \approx 2.2ER_C$ for uniform solid cells, where E is the Young's modulus of a homogeneous cellular solid. The coefficient 2.2 is experimentally determined by considering the effect of constriction wall thickness in a homogeneous half-space model.[33]

The Hagen-Poiseuille viscous pressure term[34] for a circular channel shows a 1st order behavior with respect to velocity,

$$P_{vis} = \frac{8\eta L}{r^2} u. \tag{3}$$

Here, u is the average velocity in a circular channel and r is the radius of a circular channel. Expressions for non-circular geometries can be found in Ref. 34.

Besides, the total minor loss pressure in the constriction channel shows a 2nd order relation with respect to the velocity in the constriction channel,

$$P_{C-E} = (K_E + K_C) \frac{\rho \overline{U^2}}{2}. \tag{4}$$

The energy losses of the fluid due to a sudden flow constriction and expansion can be described by the Borda-Carnot equation. According to this empirical equation, the minor loss in a pipe flow is proportional to the velocity squared, which can be expressed by $P_C = K_C(\frac{\overline{U^2}}{2g})$ and $P_E = K_E(\frac{\overline{U^2}}{2g})$. Here, $\overline{U}$ is the average velocity in the constriction and K_C and K_E are the empirical loss coefficients. They are dimensionless with values between 0 and 1. For cases when the pipe enters with very large enlargements (in our case, the enlargement ratio is 36, which is large enough), all kinetic energy in the constriction assumed to be dissipated; therefore, $K_E = 1$. Energy losses for sudden contraction are less than those for sudden enlargement, for square-edged inlet (sudden contraction with 90° vertical wall), $K_C = 0.5$. For different geometry designs, like gradual enlargement, empirical loss coefficients can be obtained from Ref. 35. Details, explanations, and applications of Eqs. (2)–(4) in the present study are summarized in Table II. Analytical estimation of these pressure terms is tabulated in Table II.

C. Impulse estimation

Based on the decomposition, the pressures are functions of the velocity inside constriction ($\overline{U}$) with an exponent raised to the i-th power, i.e., $P_i = P_i(\overline{U^i})$. The impulse of the input force experienced by the droplet is the total momentum transferred from the channel inlet into the system, which can be expressed as

$$I = \sum\nolimits_{i=0}^{2} P_i A_{ch} \Delta t. \tag{5}$$

Here, i is the index ranging over 0, 1, 2 indicating the sum of the three pressure components listed in Table II. Impulse, I, is a function of pressure terms P_i, the cross-sectional area of the un-constricted channel A_{ch} (the chamber in Fig. 2), and the impact time is used to calculate the impulse during the droplet transport: $\Delta t = t - t_0$, here we set $t_0 = 0$ as the initial contact of droplet with the channel wall.

An analytical estimation of the momentum input from the inlet to the system can be derived by inserting the equations given in Table II and Eq. (1) into Eq. (5),

$$\begin{aligned} I &= \frac{1}{2}\gamma A_f \frac{V_D + V_c}{\overline{U} A_C} \left[\overline{P}_{sur} + (K_E + K_C) \frac{\rho \overline{U^2}}{2} \right. \\ &\quad \left. + \frac{8\eta(L_C + L_{CH}/\gamma)}{R_c^2} \overline{U} \right] \\ &= \frac{1}{2}\gamma(V_D + V_c) \left[\frac{\overline{P}_{sur}}{\overline{U}} + (K_E + K_C) \frac{\rho \overline{U}}{2} \right. \\ &\quad \left. + \frac{8\eta(L_C + L_{CH}/\gamma)}{R_c^2} \right]. \end{aligned} \tag{6}$$

Here, γ is the ratio between the areas of the un-constricted and constricted regions of the channel, $\gamma = (R_{CH}/R_C)^2$. Here, R_{CH} is the radius of the un-constricted channel and γ is commonly a design constant for a specific configuration. In the numerical studies, $\gamma = 36$ under the setting of $R_{CH}/R_C = 6$.

By applying the inequality of arithmetic and geometric means (or AM–GM inequality) to the two terms, $\frac{\overline{P}_{sur}}{\overline{U}}$ and $(K_E + K_C)\frac{\rho \overline{U}}{2}$, we obtain

$$\frac{\overline{P}_{sur}}{\overline{U}} + (K_E + K_C) \frac{\rho \overline{U}}{2} \geq 2\sqrt{\overline{P}_{sur} \frac{\rho}{2} (K_E + K_C)}. \tag{7}$$

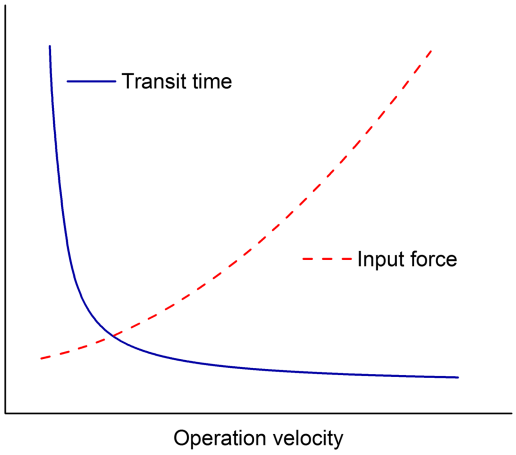

FIG. 4. Physical reason for the minimum impulse condition: a second-order input force and an inverse transit time with respect to the operation velocity.

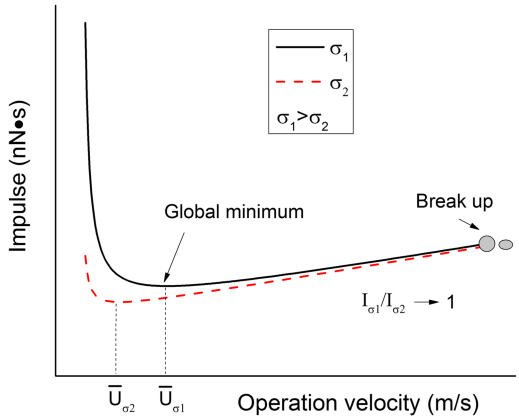

FIG. 5. Impulse-operation velocity relation when squeezing droplets with different surface tension coefficients through a circular constriction.

The global minimum of the above expression, $2\sqrt{\overline{P}_{sur}\frac{\rho}{2}(K_E+K_C)}$, is a term depending on the time-averaged pressure drop due to the surface tension, the fluid density, and the geometric shape of the constriction channel. Alternatively, these results are the same as the routine way of finding the minimum as a solution to the equation $\partial I/\partial\overline{U}=0$.

Using the relation in Eq. (7), the following analytical form of the minimum momentum change can be obtained:

$$I_{min}=\gamma(V_D+V_c)\sqrt{\overline{P}_{sur}\frac{\rho}{2}(K_E+K_C)}+const. \tag{8}$$

The minimum moment occurs when the two terms, $\frac{\overline{P}_{sur}}{\overline{U}}$ and $(K_E+K_C)\frac{\rho\overline{U}}{2}$, are equal, i.e., $\overline{P}_{sur}=(K_E+K_C)\frac{\rho\overline{U^2}}{2}$. The *const* term in Eq. (8) is induced by the viscous term along the channel with respect to the velocity change.

The physical meaning of this expression is that the droplet can be transported with the minimum momentum change when the average pressure drop due to the surface tension for the time period between 0 and $\tau/2$ equals the summation of the pressure drops due to contraction and expansion. Furthermore, there exists a critical velocity, $\overline{U}_{CR}$, such that the droplet can be transported with minimum momentum change,

$$\overline{U}_{CR}=\sqrt{\frac{2}{(K_E+K_C)}\frac{\overline{P}_{sur}}{\rho}}. \tag{9}$$

By inserting equations from Table II into Eq. (9), we get

TABLE III. Analytical estimation of relations.

Case	Operation condition	Estimation
1	$v\to 0$	$\frac{I_{\sigma 1}}{I_{\sigma 2}}=\frac{\alpha_1\sigma_1}{\alpha_2\sigma_2}$
2	$v\to 0$	$\frac{\overline{U}_{\sigma 1}}{\overline{U}_{\sigma 2}}=\sqrt{\frac{\alpha_1\sigma_1}{\alpha_2\sigma_2}}$,
3	$v\to\infty$	$\frac{I_{\sigma 1}}{I_{\sigma 2}}\to 1$

$$\overline{U}_{CR}=\sqrt{\frac{4\alpha}{(K_E+K_C)}\frac{\sigma}{\rho}\left(\frac{1}{R_C}-\frac{1}{R_D}\right)}. \tag{10}$$

By definition in Eq. (5), the impulse is the product of applied force and time. Under the continuity equation and no-gap assumption, the transit time can be expressed as an inverse relation with the operation velocity (−1st order impact) in Eq. (1). At the same time, the force term is a combination of three terms (0th, 1st, and 2nd order impact) with respect to the operation velocity as seen in Fig. 4. Consequently, the impulse is a combination of −1st, 1st order of operation velocity as well as a constant term (0th order). Under these impacts, the minimum impulse can be derived.

Besides, we also investigated the impulse of squeezing droplets with different surface tension coefficients ($\sigma_2<\sigma_1$). A collection of analytical estimations is tabulated in Table III. Table III shows the following: (1) At extremely low velocity, the ratio of impulses needed to push two droplets through the narrow constriction is proportional to the product of surface tension coefficients and the time-averaged coefficient. (2) The ratio of minimum impulse critical velocities for two different droplets is proportional to the square root of the surface tension coefficient multiplied by the time-averaged coefficient. (3) At high velocity, either viscosity loss along the channel or constriction-and-expansion loss is much larger than the surface tension term in Table II, and the impulse ratio of pushing two droplets through a narrow constriction channel is approximately 1.

To summarize, a sketch of the momentum change with respect to the operation velocity for two different droplets is illustrated in Fig. 5. In Fig. 5 a droplet break-up model[36] is labeled in the case of future applications like droplet emulsification.

IV. NUMERICAL RESULTS

A. Numerical settings

In our numerical simulations, the Volume of Fluid (VOF) method was chosen for droplet surface tracking due to its high

efficiency and flexibility for treating free boundary configurations. A 2D axis-swirl model (3D equivalent) is applied with the centerline as the axis of symmetry. A velocity inlet (with $\overline{u}$ = constant) and a pressure outlet (with gauge pressure $P_{out} = 0$) boundary conditions are applied. Detailed descriptions of this numerical approach can be found in our previous publication.[6]

Parameter settings used in the simulations are as follows. The surface tension between a non-wetting droplet and carrier fluid is σ_1 = 50 mN/m, σ_2 = 10 mN/m; the radius of the constriction is R_C = 2.5 μm; the constricted channel length is L_C = 15 μm; the radius of the un-deformed droplet is R_D = 8 μm; and the radius of un-constricted channel is R_{CH} = 15 μm. Thus $\gamma = (R_{CH}/R_C)^2 = 36$ in our simulations. In the numerical simulations, the chamber inlet velocity is the input parameter. To reproduce the simulation results easier, we used the chamber inlet velocity in the simulation result parts. The operation velocity ($\overline{U}$) in constriction is obtained indirectly through the chamber inlet velocity ($\overline{u}$). The relation between the operation velocity at chamber inlet velocity is decided by geometries, $\overline{u} = \overline{U}/36$.

To understand the state of the flow, we also labeled the Reynolds number (in the constriction), $Re = 2\rho\overline{U}R_C/\mu$. Here, ρ is the density of the carrier fluid (kg/m^3), $\overline{U}$ is the average velocity of the fluid in the constriction channel (m/s), R_C is a radius of the constriction channel (m), and μ is the dynamic viscosity of the fluid (Pa s). Two limits in our simulation are Re = 0.018 at extremely low chamber inlet velocity $\overline{u} = 10^{-4}$ and Re = 90 at extremely high chamber inlet velocity $\overline{u}$ = 0.5 m/s.

B. Time estimation

We first compared the numerical and analytical results of time estimation for a droplet passing through a constriction. Numerically, the transit time (τ) of a droplet squeezed through a constriction can be recognized and estimated by the pressure rebounding signal at the constriction exit.[6]

As shown in Fig. 6(a), Eq. (1) is a good estimation of transit time at low operation velocity. However, with the increase of operation velocity, the time difference between the analytical and numerical results becomes larger: the numerical results are bigger than the analytical estimation. The droplet passing through time increased up to 1.7 times of the analytical estimation. When the operation velocity increased to a higher value, co-flow happens.[16,37] The droplet deformation at $\tau/2$ when co-flow happens is observed in Fig. 6(b). As seen, the carrier fluid flows together with the droplet within the constriction. The carrier fluid compresses the droplet, and the radius of droplet inside the constriction reduces to $R_{c'}$ ($<R_c$). The gap between the droplet and the wall is determined by operation conditions (velocity and sizes) and droplet properties (surface tension coefficient). Our results show that the droplet needs more time to be squeezed through the constriction. The co-flow happens at $Re \approx 25$ for a droplet with σ_1 = 50 mN/m and $Re \approx 12$ for a droplet with σ_2 = 10 mN/m.

The carrier fluid narrows down the cross section of the flow path in the constriction and increases the transit time to τ',

$$\tau' = (V_D + V_C)/\overline{U}\pi R_{c'}^2. \tag{11}$$

Here, R_c' is the radius of the droplet inside the constriction when co-flow happens, R_c' decreases with the increase of operation velocity. $R_c' < R_c$ and $\tau' > \tau$ due to the co-flow compression. The droplet with a smaller surface tension coefficient can be compressed to a smaller radius R_c', causing a larger transit time τ' in Eq. (11).

C. Momentum transfer

Numerically, the impulse I_N can be calculated by multiplying the inlet cross-sectional area and the time integration of the inlet pressure outside the constriction,

$$I_N = A_{ch}\int_0^T P_{in}(\overline{u}, t)\,dt. \tag{12}$$

Figure 6(a) shows a comparison between the analytical results of Eq. (6) and the numerical results of Eq. (12). In this figure, the analytical results are calculated by the initial condition of the simulation, which provides a quick prediction. At the same time, the numerical results are calculated by the output data of VOF simulation. The pressure curve is integrated in accordance with Eq. (12) below the P_{in} curve between 0 and $\tau/2$. As shown in Fig. 6(a), the analytical momentum change prediction is a good estimation at low velocity. However, with the increase of operation velocity, more inputs are used to elongate the droplet: either pressure demonstrated in previous studies[16] or transit time demonstrated in Fig. 6(a) in the present study. Consequently, the momentum change in numerical results is larger than the simplified theoretical

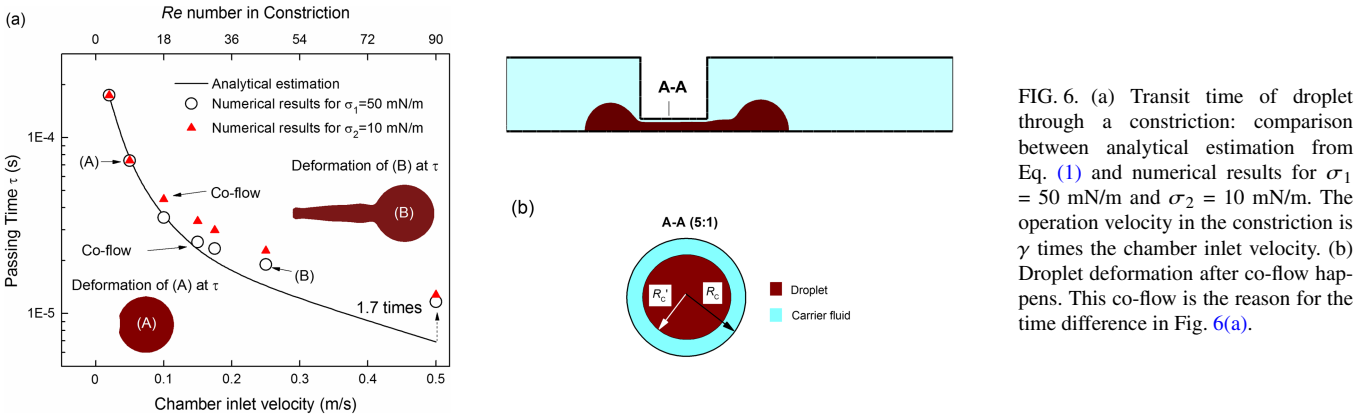

FIG. 6. (a) Transit time of droplet through a constriction: comparison between analytical estimation from Eq. (1) and numerical results for σ_1 = 50 mN/m and σ_2 = 10 mN/m. The operation velocity in the constriction is γ times the chamber inlet velocity. (b) Droplet deformation after co-flow happens. This co-flow is the reason for the time difference in Fig. 6(a).

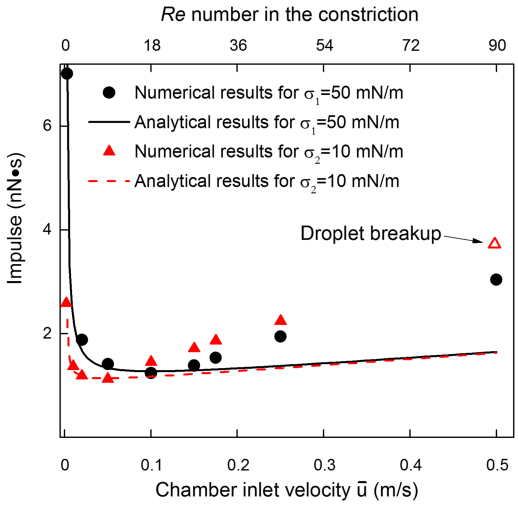

FIG. 7. Impulse of droplet passing through a constriction for a droplet with surface tension $\sigma_1 = 50$ mN/m and respectively $\sigma_2 = 10$ mN/m. The operation velocity in constriction is γ times the chamber inlet velocity.

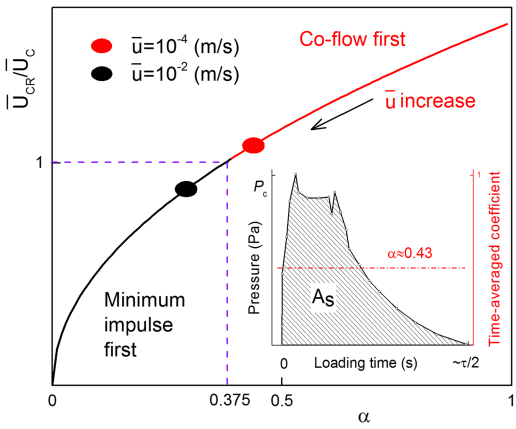

FIG. 8. The ratio of minimum impulse critical velocity and co-flow critical velocity, $\overline{U}_{CR}/\overline{U}_C$. The inset with $\alpha = 0.43$ at the right bottom corner is a loading curve at the extremely slow velocity, $\bar{u} = 10^{-4}$ (m/s). It is used to demonstrate how to calculate the time-averaged coefficient. The time-averaged coefficient is defined as $\alpha = A_S/(P_{CR} * \tau/2)$, where A_S is the area between P_{in} and the viscous loss curve ($P_{vis} + P_{C-E}$).

prediction of Eq. (2). Besides, the momentum change for $\sigma_2 = 10$ mN/m may become larger than $\sigma_1 = 50$ mN/m cases at high operation velocity due to the transit time difference when co-flow happens in Fig. 6(b). Lastly, the droplet breakup is also observed at the high speed operation condition for droplet with $\sigma_2 = 10$ mN/m.

As seen in Fig. 7, with the increase of operation velocity, the impulse needed to push through the droplet first decreases to the minimum at $\overline{U}_{CR}$ and then increases. The impulse difference between the analytical and numerical results is caused by three reasons: (1) the increased transit time (τ') described in Eq. (11) increased the time duration term in Eq. (1); (2) the droplet elongation needs extra time as seen in Fig. 6(a); (3) as the operation velocity grows larger than $\overline{U}_C$, the surface tension term decreases as previously described in Ref. 16. These three influence factors are difficult to be implanted in the analytical model.

For the analytical estimation in Table III, if $\sigma_2 < \sigma_1$, the numerical result shows $\frac{I_{\sigma 1}}{I_{\sigma 2}} < \frac{\sigma_1}{\sigma_2}$ since we found that the time-averaged coefficient (α_1) decreases with the increase of operation velocity. For example, for two droplets with the surface tension of $\sigma_1 = 50$ mN/m and $\sigma_2 = 10$ mN/m, the ratio of impulses at extremely low velocity (0.002 m/s) is $I_{\sigma 1}/I_{\sigma 2} \approx 3.7 (< \sigma_1/\sigma_2 = 5)$. Estimation for the case at $v \to \infty$ is also influenced due to co-flow and droplet breakup.

D. Critical velocity ratio

We notice the difference between the minimum impulse critical velocity in Eq. (10) and the co-flow critical velocity $\overline{U}_C = \sqrt{\frac{\sigma}{\rho}(\frac{1}{R_C} - \frac{1}{R_D})}$, previously defined in Ref. 16 by balancing the surface tension, shear stress, and dynamic pressure using a lubrication model (assuming the thickness of the gap between the interface of droplet and channel wall is small enough comparing with the radius of the constriction). We can see that the minimum impulse critical velocity obtained in this paper is $\sqrt{\frac{4\alpha}{K_E + K_C}}$ times the co-flow critical velocity $\overline{U}_C$, i.e.,

$$\overline{U}_{CR}/\overline{U}_C = \sqrt{\frac{4\alpha}{K_E + K_C}}. \tag{13}$$

This ratio can tell whether the minimum impulse transportation happens first or co-flow happens first. Mathematically, if $\alpha < 0.375$, $\overline{U}_{CR}$ happens before $\overline{U}_C$. Otherwise, co-flow happens before the minimum impulse transport. For a sudden contraction-and-expansion channel configuration with $K_E + K_C = 1.5$, as a rule of thumb, if $\alpha < 0.375$ at an operation velocity lower than the co-flow critical velocity, the minimum impulse transportation happens first because we found that α decreases with the increase of operation velocity. For example, as shown in Fig. 8 for the case of a droplet with surface tension coefficient $\sigma = 50$ mN/m, when the chamber inlet velocity ($\bar{u}$) increases from 10^{-4} m/s to 10^{-2} m/s, α decreases from 0.43 to 0.33. Since the critical velocity happens at a $\bar{u}$ much larger than 10^{-2} m/s, we can get the conclusion that the minimum impulse transport happens before the co-flow critical velocity.

V. CONCLUSION

In the present research, we focused on the impulse of squeezing a droplet through a narrow circular constriction. An analytical model of squeezing a droplet through a circular constriction is built. By averaging the surface tension term, we found a condition for the minimum impulse transport analytically. The corresponding critical velocity and impulse transport condition were defined and expressed. The analytical results were compared with numerical studies performed using the volume of fluid method. Results show that the analytical model performs well at low velocity before the critical velocity is reached in both time estimation and impulse estimation, but underestimates the impulse at higher velocities after co-flow happens. We believe that this minimum impulse transport condition has the potential to be widely applied in optimization problems of interest in biology, lab on a chip,

or chemical engineering such as the design of micro-filters or multiphase nozzles.

ACKNOWLEDGMENTS

Zhifeng Zhang thanks the support of Robert A. Sebrisky Fellowship awarded by the Department of Engineering Science and Mechanics, at the Pennsylvania State University, and the inspiring environment provided by the Dissertation Boost Camp at the Pennsylvania State University.

NOMENCLATURE

A_c	Cross-sectional area of constriction (m^2)
A_{ch}	Cross-sectional area of un-constricted channel (m^2)
A_S	Surface tension induced loading (Pa s)
E	Young's modulus (Pa)
L_c	Length of constriction channel (m)
L_{ch}	Length of un-constricted channel (m)
r	Radius of a circular channel (m)
R_C	Droplet radius inside the constriction before co-flow happens (m)
	Radius of constriction channel (m)
$R_{C'}$	Reduced radius of droplet in the constriction after co-flow happens (m)
R_D	Radius of un-deformed droplet (m)
R_{ch}	Radius of un-constricted channel (m^2)
Re_c	Reynolds number in the constriction channel (-)
K_E	Expansion coefficient (-)
K_C	Constriction coefficient (-)
$\overline{U}$	Operation velocity, velocity in the constriction (m/s)
$\overline{u}$	Chamber inlet velocity, velocity in the un-constricted channel (m/s)
$\overline{U}_{CR}$	Minimum impulse critical velocity (m/s)
$\overline{U}_C$	Co-flow critical velocity (m/s)
u	Velocity in a circular channel (m/s)
P_i	i-th order of impact with respect to velocity (Pa)
P_{in}	Inlet pressure (Pa)
P_{surf}	Dynamic surface tension (Pa)
P_{CR}	Critical surface tension (Pa)
P_{vis}	Viscous pressure loss (Pa)
T	Characteristic impact time (s)
Δt	Impact time (s)
I	Impulse (N s)
I_σ	Impulse for droplet with a specific surface tension (N s)
I_N	Impulse from numerical results (N s)
V_T	The total volume of fluid transported (m^3)
V_C	Volume of constriction (m^3)
V_D	Volume of droplet (m^3)
σ	Surface tension coefficient (N/m)
σ_{eq}	Equivalent surface tension coefficient (N/m)
τ	Droplet transit time (s)
τ'	Droplet transit time after co-flow happens (s)
α	Time-averaged coefficient (-)
ρ	Density of fluid (kg/m^3)
γ	Chamber-constriction area ratio (-)
η	Dynamic viscosity of fluid (Pa s)

[1] S. H. Au, B. D. Storey, J. C. Moore, Q. Tang, Y.-L. Chen, S. Javaid, A. F. Sarioglu, R. Sullivan, M. W. Madden, R. O'Keefe *et al.*, "Clusters of circulating tumor cells traverse capillary-sized vessels," Proc. Natl. Acad. Sci. U. S. A. **113**, 4947 (2016).
[2] J. P. Shelby, J. White, K. Ganesan, P. K. Rathod, and D. T. Chiu, "A microfluidic model for single-cell capillary obstruction by *Plasmodium* falciparum-infected erythrocytes," Proc. Natl. Acad. Sci. U. S. A. **100**, 14618 (2003).
[3] D. M. Wootton and D. N. Ku, "Fluid mechanics of vascular systems, diseases, and thrombosis," Annu. Rev. Biomed. Eng. **1**, 299 (1999).
[4] R. M. Hochmuth, "Micropipette aspiration of living cells," J. Biomech. **33**, 15 (2000).
[5] J. Lee, A. Sharei, W. Y. Sim, A. Adamo, R. Langer, K. F. Jensen, and M. G. Bawendi, "Nonendocytic delivery of functional engineered nanoparticles into the cytoplasm of live cells using a novel, high-throughput microfluidic device," Nano Lett. **12**, 6322 (2012).
[6] Z. Zhang, J. Xu, B. Hong, and X. Chen, "The effects of 3D channel geometry on CTC passing pressure–towards deformability-based cancer cell separation," Lab Chip **14**, 2576 (2014).
[7] G. R. Hendrickson and L. A. Lyon, "Microgel translocation through pores under confinement," Angew. Chem., Int. Ed. **49**, 2193 (2010).
[8] S. Cobos, M. Carvalho, and V. Alvarado, "Flow of oil–water emulsions through a constricted capillary," Int. J. Multiphase Flow **35**, 507 (2009).
[9] Y. S. Polyakov and A. L. Zydney, "Ultrafiltration membrane performance: Effects of pore blockage/constriction," J. Membr. Sci. **434**, 106 (2013).
[10] I. A. Beresnev and W. Deng, "Viscosity effects in vibratory mobilization of residual oil," Geophysics **75**, N79 (2010).
[11] C. Zhou, P. Yue, and J. J. Feng, "Deformation of a compound drop through a contraction in a pressure-driven pipe flow," Int. J. Multiphase Flow **34**, 102 (2008).
[12] Z. Zhang, J. Xu, and X. Chen, *Compound Droplet Modelling of Circulating Tumor Cell Microfiltration* (American Society of Mechanical Engineers, 2015).
[13] J. Berthier and K. Brakke, *The Physics of Microdroplets* (John Wiley & Sons, 2012).
[14] M. Liang, S. Yang, T. Miao, and B. Yu, "Minimum applied pressure for a drop through an abruptly constricted capillary," Microfluid. Nanofluid. **19**, 1 (2015).
[15] Z. Zhang, X. Zhao, J. Xu, and X. Chen, "The critical velocity with minimum momentum change in pushing a droplet through a constriction channel," in *ASME 2016 International Mechanical Engineering Congress and Exposition* (American Society of Mechanical Engineers, 2016), pp. V007T09A055.
[16] Z. Zhang, X. Chen, and J. Xu, "Entry effects of droplet in a micro confinement: Implications for deformation-based circulating tumor cell microfiltration," Biomicrofluidics **9**, 024108 (2015).
[17] M. Aghaamoo, Z. Zhang, X. Chen, and J. Xu, "Deformability-based circulating tumor cell separation with conical-shaped microfilters: Concept, optimization, and design criteria," Biomicrofluidics **9**, 034106 (2015).
[18] Z. Zhang, J. Xu, and X. Chen, *Predictive Model for the Cell Passing Pressure in Deformation-Based CTC Chips* (American Society of Mechanical Engineers, 2014).
[19] E. Benet and F. J. Vernerey, "Mechanics and stability of vesicles and droplets in confined spaces," Phys. Rev. E **94**, 062613 (2016).
[20] Y. Li and T. Tanaka, "Kinetics of swelling and shrinking of gels," J. Chem. Phys. **92**, 1365 (1990).
[21] R. Kusters, T. van der Heijden, B. Kaoui, J. Harting, and C. Storm, "Forced transport of deformable containers through narrow constrictions," Phys. Rev. E **90**, 033006 (2014).
[22] T. Wu, Q. Guo, H. Ma, and J. J. Feng, "The critical pressure for driving a red blood cell through a contracting microfluidic channel," Theor. Appl. Mech. Lett. **5**, 227 (2015).
[23] Z. Luo, S. Güven, I. Gozen, P. Chen, S. Tasoglu, R. M. Anchan, B. Bai, and U. Demirci, "Deformation of a single mouse oocyte in a constricted microfluidic channel," Microfluid. Nanofluid. **19**, 883 (2015).
[24] J. P. Arata and A. Alexeev, "Designing microfluidic channel that separates elastic particles upon stiffness," Soft Matter **5**, 2721 (2009).
[25] F. Y. Leong, Q. Li, C. T. Lim, and K.-H. Chiam, "Modeling cell entry into a micro-channel," Biomech. Model. Mechanobiol. **10**, 755 (2011).
[26] H. C. Kan, H. S. Udaykumar, S. Wei, and R. Tran-Son-Tay, "Hydrodynamics of a compound drop with application to leukocyte modeling," Phys. Fluids **10**, 760 (1998).

[27]X. Li, Z. Peng, H. Lei, M. Dao, and G. E. Karniadakis, "Probing red blood cell mechanics, rheology and dynamics with a two-component multi-scale model," Philos. Trans. R. Soc., A **372**, 20130389 (2014).
[28]M. Wörner, "Numerical modeling of multiphase flows in microfluidics and micro process engineering: A review of methods and applications," Microfluid. Nanofluid. **12**, 841 (2012).
[29]C. W. Hirt and B. D. Nichols, "Volume of fluid (VOF) method for the dynamics of free boundaries," J. Comput. Phys. **39**, 201 (1981).
[30]A. Leyrat-Maurin and D. Barthes-Biesel, "Motion of a deformable capsule through a hyperbolic constriction," J. Fluid Mech. **279**, 135 (1994).
[31]T. W. Secomb, R. Skalak, N. Özkaya, and J. Gross, "Flow of axisymmetric red blood cells in narrow capillaries," J. Fluid Mech. **163**, 405 (1986).
[32]C. Rorai, A. Touchard, L. Zhu, and L. Brandt, "Motion of an elastic capsule in a constricted microchannel," Eur. Phys. J. E **38**, 49 (2015).
[33]D. P. Theret, M. J. Levesque, M. Sato, R. M. Nerem, and L. T. Wheeler, "The application of a homogeneous half-space model in the analysis of endothelial cell micropipette measurements," J. Biomech. Eng. **110**, 190 (1988).
[34]H. Bruus, *Theoretical Microfluidics* (Oxford University Press, 2008).
[35]R. L. Mott, F. M. Noor, and A. A. Aziz, *Applied Fluid Mechanics* (Pearson Prentice Hall, Singapore, 2006).
[36]L. Rosenfeld, L. Fan, Y. Chen, R. Swoboda, and S. K. Y. Tang, "Break-up of droplets in a concentrated emulsion flowing through a narrow constriction," Soft Matter **10**, 421 (2014).
[37]Z. Zhang, J. Xu, and X. Chen, *Modeling Cell Deformation in CTC Microfluidic Filters* (American Society of Mechanical Engineers, 2014).